Surface Domain Structures and Mesoscopic Phase Transition in Relaxor Ferroelectrics

Andrei Kholkin, Anna Morozovska, Dmitry Kiselev, Igor Bdikin, Brian Rodriguez, Pingping Wu, Alexei Bokov, Zuo-Guang Ye, Brahim Dkhil, Long-Qing Chen, Marija Kosec, and Sergei V. Kalinin**

Relaxor ferroelectrics are a prototypical example of ferroic systems in which interplay between atomic disorder and order parameters gives rise to emergence of unusual properties, including non-exponential relaxations, memory effects, polarization rotations, and broad spectrum of bias- and temperature-induced phase transitions. Despite more than 40 years of extensive research following the original discovery of ferroelectric relaxors by the Smolensky group, the most basic aspect of these materials – the existence and nature of order parameter – has not been understood thoroughly. Using extensive imaging and spectroscopic studies by variable-temperature and time resolved piezoresponse force microscopy, we find that the observed mesoscopic behavior is consistent with the presence of two effective order parameters describing dynamic and static parts of polarization, respectively. The static component gives rise to rich spatially ordered systems on the ~100 nm length scales, and are only weakly responsive to electric field. The surface of relaxors undergoes a mesoscopic symmetry breaking leading to the freezing of polarization fluctuations and shift of corresponding transition temperature.

1. Introduction

Disordered systems including magnetic spin and cluster glasses,[1] ferroelastic martensites,[2] dipolar and quadrupolar glasses,[3] ferroelectric relaxors,[4] structural glasses,[5] as well as more exotic matter such as vortex lattices in superconductors[6] have remained a focus of extensive theoretical and experimental effort over the last 5 decades. This interest is precipitated by the unique properties emerging as a result of disorder interaction with order parameter field, including high magnetic and electromechanical coupling constants, tunability of dielectric and magnetic responses, as well as unique memory effects. By now, many of the theoretical concepts formulated on the quest to understand the physics of disordered systems, such as Edwards–Anderson models for spin glasses[1] and spherical random bond-random field model for relaxors,[7] have become the bedrock of statistical physics.

Ferroelectric relaxors are a prototypical example of disordered ferroic systems. These materials have been originally discovered by Smolensky and co-workers in 1954[8,9] and were believed to undergo unusual diffuse phase transitions associated with the broad

Dr. A. Kholkin, Dr. D. Kiselev
Department of Ceramic and Glass Engineering & CICECO
University of Aveiro
3810–193 Aveiro, Portugal
E-mail: kholkin@ua.pt
Dr. A. Morozovska
Institute of Semiconductor Physics
National Academy of Science of Ukraine
03028 Kiev, Ukraine
Dr. I. Bdikin
Centre for Mechanical Technology and Automation
University of Aveiro
3810–193 Aveiro, Portugal
Dr. B. Rodriguez
Conway Institute of Biomolecular and Biomedical Research
University College Dublin
Belfield, Dublin 4, Ireland
P. Wu, L.-Q. Chen
Department of Materials Science and Engineering
The Pennsylvania State University
University Park
PA, 16802, USA
Dr. A. Bokov, Prof. Z.-G. Ye
Department of Chemistry and 4D LABS
Simon Fraser University
Burnaby, British Columbia, V5A 1S6, Canada
Prof. B. Dkhil
Laboratoire Structure
Propriétés et Modélisation des Solides
UMR CNRS 8580, Ecole Centrale Paris
92295 Chatenay-Malabry Cedex, France
Prof. M. Kosec
Jozef Stefan Institute
1000 Ljubljana, Slovenia
Dr. S. V. Kalinin
The Center for Nanophase Materials Sciences
and Materials Sciences and Technology Division
Oak Ridge National Laboratory
Oak Ridge, TN 37831
E-mail: sergei2@ornl.gov

DOI: 10.1002/adfm.201002582

and frequency dispersive variations of dielectric permittivity as a function of temperature. The origins of these behaviors were traced to the presence of polar nanoregions of typically 1–5 nm size,[10] the dynamics of which underpins relaxor properties. The resurgence of interest in relaxors in the last decades is largely related to applications including ultrasonic medical and underwater imaging,[11,12] as well as progress in theoretical concepts.[13] Relaxors have been extensively studied using macroscopic time-resolved spectroscopies, including a broad range of phenomena from non-exponential relaxations common for disordered systems,[14] to complex dynamic phenomena such as spectral hole burning[15] and memory effects.[16] Significant progress in atomistic understanding of relaxors has been achieved using model Hamiltonian, density-functional theory,[17] and optical,[18] neutron[19] and x-ray scattering.[20] Despite the progress, many aspects of mesoscopic relaxor physics are still unresolved, including the existence and nature of order parameter, the mechanisms of PNR reorientation, and the nature of bias- and temperature-induced phase transitions.

The challenge in studies of disordered systems has traditionally been the difficulty in acquiring the spatially resolved information. We note that ferroelectric relaxors provide a convenient model system, in which the local dipole reorientation does not change the underlying crystallographic lattice, and hence is (potentially) reversible. At the same time, the strong coupling between polarization and strain (reversible lattice deformation) allows the polarization dynamics to be studied. Here, we present the results of mesoscopic studies of ferroelectric relaxors using temperature- and time-resolved piezoresponse force microscopy, which reveal the mechanisms of temperature- and bias-induced phase transitions and suggest the complex nature of order parameters containing at least two components.

2. Results and Discussion

2.1. Time and Voltage Dynamics of Polarization in Relaxors

As model systems, we have chosen two representatives of the most investigated relaxor families, namely the ceramics of La-doped lead zirconate-titanate solid solution ($Pb_{1-x}La_xZr_{0.65}Ti_{0.35}O_3$, with x = 8% and 9.5%, abbreviated hereafter as PLZT-8% and PLZT-9.5%)[21] and the single crystals of lead-zinc-niobate – lead titanate solid solution ($0.955PbZn_{1/3}Nb_{2/3}O_3$ -$0.045PbTiO_3$, PZN-4.5%PT).[22] The ceramic materials contain well-defined grains that serve as convenient topographic markers for depth sectioning and variable temperature experiments, and allow us to study the universality of behaviors for different crystallographic orientations. In comparison, PZN-4.5%PT crystals of (100) and (111) facets offer the advantage of known crystallographic orientation for well-defined material. However, most of the observed behaviors have been found also in other relaxor systems such as PMN-PT[23–27] suggesting the observed phenomena are universal for relaxor materials in general.

The imaging has been performed using piezoresponse force microscopy (PFM).[28,29] In PFM, a biased conductive tip probe concentrates an electric field to a nanoscale volume of material (~10–30 nm) and the measured electromechanical response

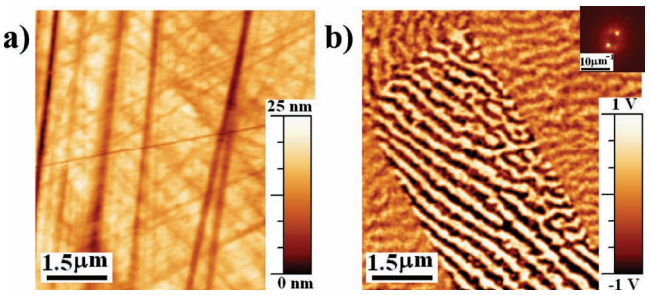

Figure 1. a) Surface topography and b) piezoresponse force microscopy images of PLZT-9.5% ceramics. Inset shows a 2D FFT of corresponding PFM image.

provides information on local polarization. In switching[30] and spectroscopic experiments,[31,32] application of a dc bias results in polarization switching below the probe and the resulting change in polar structure can be determined as subsequent imaging (switching experiment) or as a change in ac response (spectroscopic mode). The details of materials preparation, full range of studied systems, and experiment are presented in Experimental Section.

The typical surface topography and PFM images at room temperature of PLZT-9.5% ceramics are shown in **Figure 1**. The system clearly illustrates labyrinthine domain pattern with well-defined characteristic length scale visible as a ring on the corresponding Fourier transform.[33] Note that, while fractal domain structures are often observed for relaxor compositions close to relaxor-ferroelectric boundary,[34,35] the labyrinthine patterns observed for these compositions are consistent with the presence of a single characteristic length scale (similar to domain structure). Depending on the grain orientation, both transversally-isotropic pattern (e.g. similar to those observed in ultrathin magnetic films[36]) and preferential pattern orientations are observed.[37] These were also found to depend on the position within the grain.[38] Furthermore, recent focused X-ray studies on similar compositions[35] demonstrate that the deviation from cubic symmetry is negligible, suggesting that lattice distortion associated with labyrinthine structures is small. Note that in the systems closer to ferroelectric limit, these labyrinthine structures roughen and can coexist with classical ferroelectric domains.[39,40]

To establish the mechanism controlling polarization dynamics, tip-induced switching experiments with subsequent depth analysis were performed. Shown in **Figure 2** are the results of the poling experiment on the surface with labyrinthine pattern. In classical ferroelectrics, tip-induced switching results in formation of localized domain with well-saturated polarization, i.e., switching proceeds through formation of well-defined area within which polarization switched form state $-P$ to P. The resulting domain can be metastable, and will relax through radial shrinking, albeit maintaining the same phase state in the core.[41–45] In comparison, the polarization switching in relaxors shows a number of remarkable behaviors. Switching proceeds through formation of domains within the scanned region, however the signal within the domain scales with the writing voltage (as opposed to an increase of the effective domain size). The magnitude of switched contrast is an order of magnitude higher than the contrast of pre-existing labyrinth

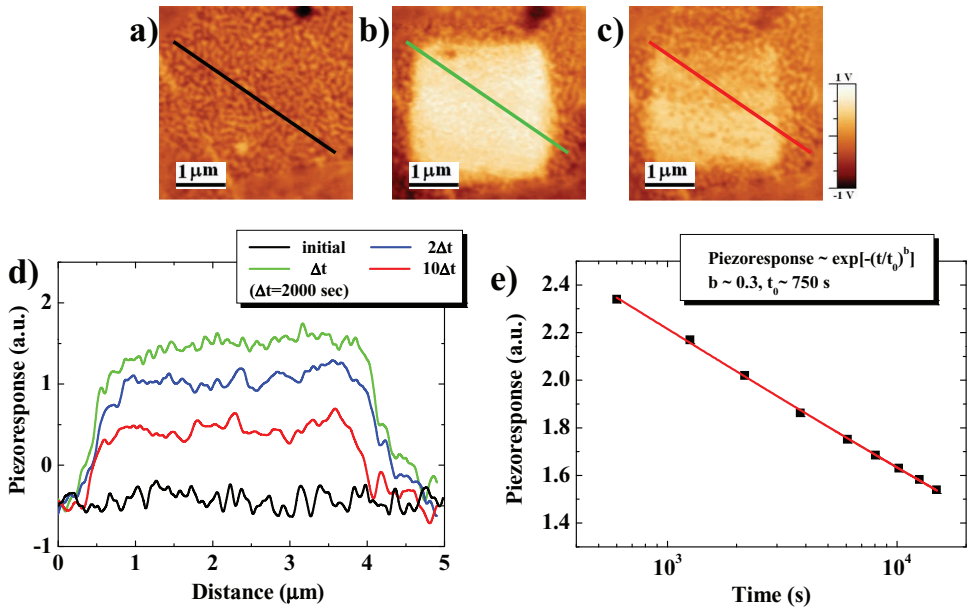

Figure 2. Piezoresponse force microscopy images of a) pristine PLZT-9.5% surface, b) surface immediately after domain writing, and c) after relaxation during 5.5 hours; d) the corresponding profiles averaged over 50 lines. Note that, unlike classical ferroelectrics in which relaxation proceeds by domain wall motion, in relaxors contrast fades uniformly with time. Furthermore, the switchable polarization and polarization wave coexist in the switched region, and the wave is unaffected by switching.

structures. Most strikingly, the labyrinthine domains are not affected by the bias pulse, and are clearly visible on top of the induced polarization pattern. The reverse process is observed in the bias-off state, when induced polarization relaxes with time. Unlike in classical ferroelectrics, the polarization decays almost uniformly within the switched area, rather than through lateral contraction of this area. The relaxation law follows a stretched exponential behavior. Notably, the labyrinthine domains emerge unaltered when the relaxation is finished.

To get insight into the mechanism of the tip-induced polarization switching and explore the topology of the ferroelectric domains in 3D, the preexisting domain structure and tip-induced domain were probed by depth sectioning experiments. In these, the domain structure was imaged by PFM in the vicinity of the grain boundary that serves as a convenient topographic reference mark. Subsequently, the surface is progressively polished and the amount of removed material is determined from the relative change of the depth of topographic features (polishing scratches). Subsequently, the polishing and imaging step is repeated. It was verified that polishing does not disturb the existing domains and domain structure is stable within the time required to perform imaging. While the topographic alignment is imperfect, the partial information can be recovered. Shown in **Figure 3**a is the result of the cross-section experiment on the pristine PLZT surface. The grain boundary (shown by dotted line) and the evolution of the domain structure around it can be clearly seen. From comparison of the images in Figure 3a in regions A and B, the domain structure changes only weakly with depth of the material, suggesting that the domain walls are oriented normal to the surface. It should be noted that the evolution of domain structure is followed in this work only down to 50–60 nm. Detailed cross-sectional experiments and their discussion are reserved for the separate publication.[46]

Similar studies for the electrically induced domain are shown in Figure 3b. Arguably, the relaxation of induced polarization pattern during polishing is possible; however, the observed pattern suggests the progressive narrowing of the induced domain with depth (as opposed to almost uniform relaxation in the surface as illustrated in Figure 2). Overall, this cross-sectioning experiment demonstrates that induced polarization pattern is concentrated in the very thin (~20 nm) near-surface layer and does not penetrate deep into the material. This

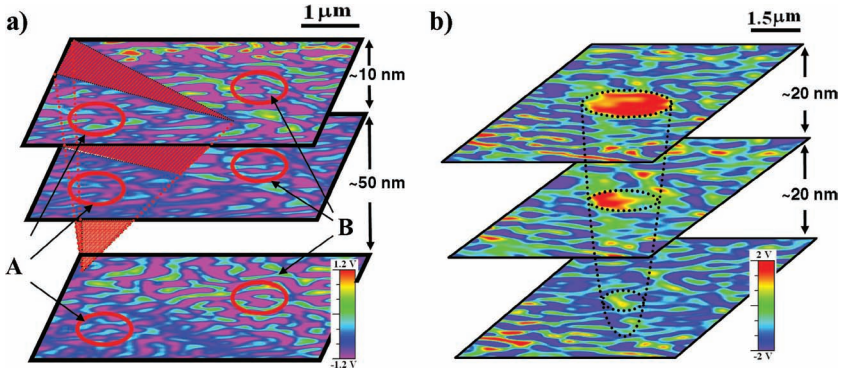

Figure 3. a) Depth sections of periodic structures illustrating depth evolution of the domains that penetrate the material. b) Depth profiling of switched region illustrating that the tip-induced domain is very shallow, unlike needle-like domains in classical ferroelectrics. Both measurements are done on PLZT-9.5% ceramics.

behavior is opposite to that of classical ferroelectrics, in which the formation of needle-like domains driven by depolarization fields is universal for uniform field[47] and PFM-induced switching.[48–50]

These observations draw a very unusual mesoscopic picture of ferroelectric relaxors in nominally ergodic state; instead of random fractal polarization distribution, a presence of characteristic mesoscopic length scale associated with non-switchable domains that extend normal to the sample surface. The switchable polarization is spatially uniform, does not penetrate deep into the material, and can correspond to the second (dynamic) component of the order parameter. It is assumed that the static and dynamic components interact only weakly. Note that while a number of authors reported the presence of micrometer-thick surface layers on relaxor surfaces,[51] our previous studies[23] have demonstrated that labyrinthine structures can exist even on nominally cubic surfaces. Furthermore, the data in Figure 3a suggest that surface layer is associated with the slight change in morphology of the labyrinthine domains, but not their absence.

2.2. Variable Temperature Studies of Polarization Dynamics

To get insight into the temperature-dependent polarization behavior including dynamic and static polarization components, both spectroscopic and imaging studies were performed as a function of temperature. These studies are complementary to hot-stage TEM observations in relaxors as reported by several authors.[52,53]

Shown in **Figure 4**a are the temperature-dependent macroscopic polarization-field (*P-E*) hysteresis loops for the polycrystalline PLZT-8% sample. At room temperature, the material exhibits classical ferroelectric-like shaped loops. On increasing the temperature to 57 °C, the loop develops constrictions, similar to the shape expected for antiferroelectric materials (e.g. for FE-AFE transition in $BiFeO_3$)[54] or ferroelectric above corresponding Curie temperature.[55] On further increasing temperature, the hysteresis loop becomes progressively slimmer (at 77 °C), and eventually evolves to almost a straight line at 127 °C. The observed evolution of hysteresis loop with temperature is somewhat similar to ferroelectric material on crossing the Curie temperature. The loop shape at 57 °C and above suggests that the zero-field phase is non-polar, but application of the finite bias promotes the polar phase that is kinetically stabilized.

To compare the bulk and surface behavior, the evolution of switchable polarization is studied by PFM spectroscopy (PFS), providing a local analog of the piezoelectric hysteresis loops. At room temperature, the loops are well saturated, indicative of the onset of completely switched state. The response on the return branch is constant and the nucleation bias is well defined, indicating that the switched state is stable for more than time scale of loop acquisition (~5 min). On increasing the temperature, the loops become progressively shrunk in the vertical direction, indicative of decrease of switchable polarization. However, the overall loop shape including almost flat return branches and well-defined nucleation biases, remains almost the same. This behavior is in drastic contrast to that in macroscopic

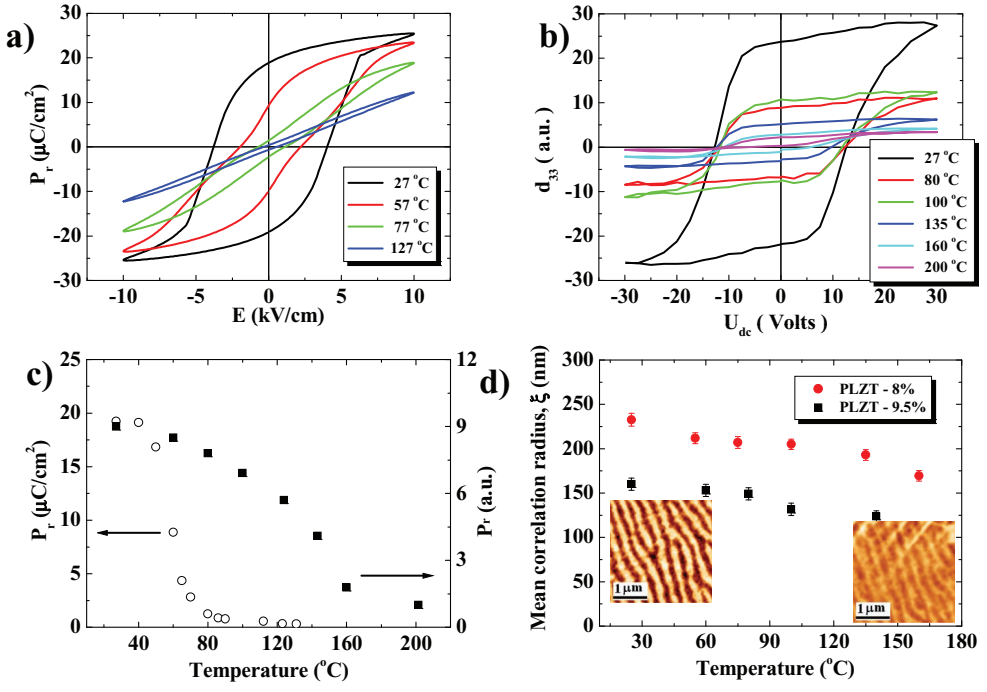

Figure 4. a) Macroscopic P-E hysteresis loops in PLZT-8% ceramics illustrating disappearance of switchable polarization at 127 °C, b) Local PFM hysteresis loops showing the persistence of switchable polarization up to 200 °C, i.e., 100 degrees above the bulk transition for PLZT-8% ceramics, c) Temperature dependence of polarization in macroscopic and local measurements in PLZT 8/65/35 ceramics, and d) periodicity of the periodic domain patterns. The insets present domain images for PLZT-9.5% at 30 °C and 120 °C, respectively. Note that domain ripples disappear simultaneously with switchable polarization, suggesting the presence of coupled mesoscopic surface phase transition.

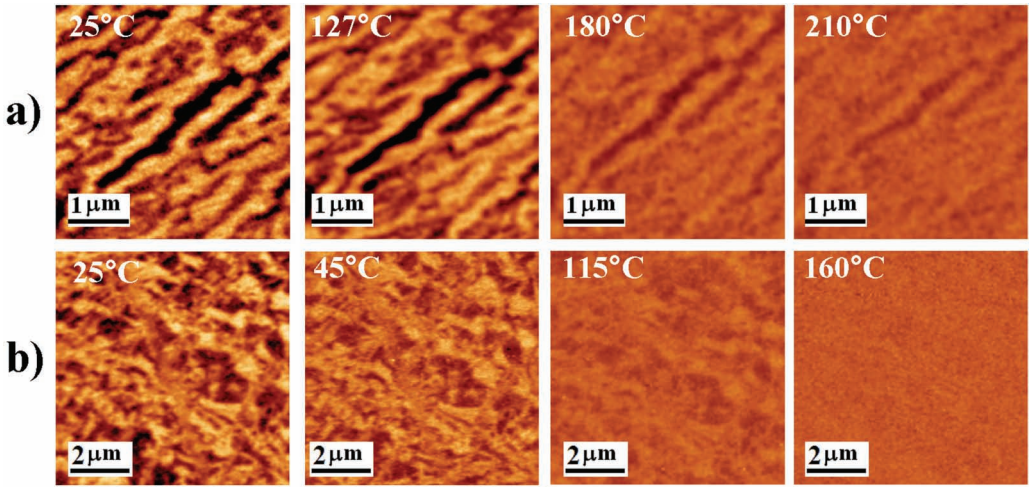

Figure 5. Evolution of surface domain structures in PZN-4.5%PT single crystals for a) (100) and b) (111) orientations. Note the difference in domain pattern morphologies and persistence of domain patterns for much higher temperatures in (100) orientation.

measurements, and differs appreciably from that of PFS of normal ferroelectrics in which the nucleation bias decreases with temperature.[56]

The remanent (zero-field) hysteretic responses for the *P-E* and PFS loops are compared in Figure 4c. Note that the bulk polarization exhibits very rapid decay with temperature (resembling that for the first order phase transition in the presence of defects) with a relatively small high-temperature tail. At the same time, the PFS signal extends much further in the high-temperature domain. From the comparison of data in Figure 4c, it can be induced that the surface tip-induced polarization can exist at temperatures almost 100 °C above the bulk transition temperature (around 100 °C).

The evolution of domain structure during the variable temperature measurements illustrates that the domain pattern remains almost invariant and no reconfiguration of the static labyrinthine domain patterns is observed. The small decrease of relevant correlation length as shown in Figure 4d can be explained by the decrease in image contrast and increase in noise. In this way, the domain relative contrast becomes smaller with temperature, following the decay of switchable polarization.

To get additional insight into the temperature dependence of static and dynamic polarization and establish the role of crystallographic orientation, similar measurements were performed on PZN-4.5%PT (100) and (111) surfaces. The temperature evolution of domain pattern is shown in **Figure 5**. For (100) termination, extended domains oriented in the general <011> direction are observed. For (111) termination, the domains are much smaller and form mosaic-like pattern. In both cases, on increasing temperature, the domain morphology remains invariant, while the associated contrast slowly decreases for large domains. For both materials domains exist above the temperature of maximum dielectric constant and structural phase transition in PZN-4.5%PT.

The temperature dependent morphological and spectroscopic studies are summarized in **Figure 6**. Similarly to PLZT, the correlation length for PZN-4.5%PT depends on the temperature relatively weakly and this dependence can be (partially) attributed to the decay of the image contrast with temperature. In comparison, the static polarization component (i.e., the amplitude of the PFM contrast in labyrinthine structures) shows more complex temperature dependence, with rapid decreases at ~45 °C for (111) surface and ~130 °C for (100) surface and a high-temperature tail above. The behavior of the dynamic polarization component is illustrated in Figure 6c,d. For (111) orientation, the remanent polarization disappears at ~90 °C. The corresponding nucleation bias (i.e., the measure of energy for nucleating the polar phase) and coercive voltage decrease with temperature and become zero at the same temperature. At the same time, for (100) termination, both remanent dynamic polarization and non-zero switching bias persist to much higher temperature.

These observations clearly illustrate that both static and dynamic components of polarization in relaxors are strongly affected by surface termination, in agreement with studies by Ozgul et al.[57] While the full explanation of the observed phenomena clearly requires more extensive structural studies, it was believed that the polarization correlations in PMN and similar materials develop in the (111) orientations.[58] Correspondingly, on the (111) surfaces there are two possible up and down orientations that couple strongly to the normal electric fields (either due to the tip, or due to the surface terminations), and 6 components with much smaller normal polarization component. At the same time, on the (100) surfaces 4 equivalent up-oriented and 4 down-oriented polarization components are degenerate. Correspondingly, the near-surface electric fields can lift the degeneracy of possible polarization states for (111) orientation, while it is not the case for (100) termination.

2.3. Phenomenological Description

The observed mesoscopic behavior is consistent with the presence of the frozen and switchable polarization components. The order parameters demonstrate similar thermal behavior

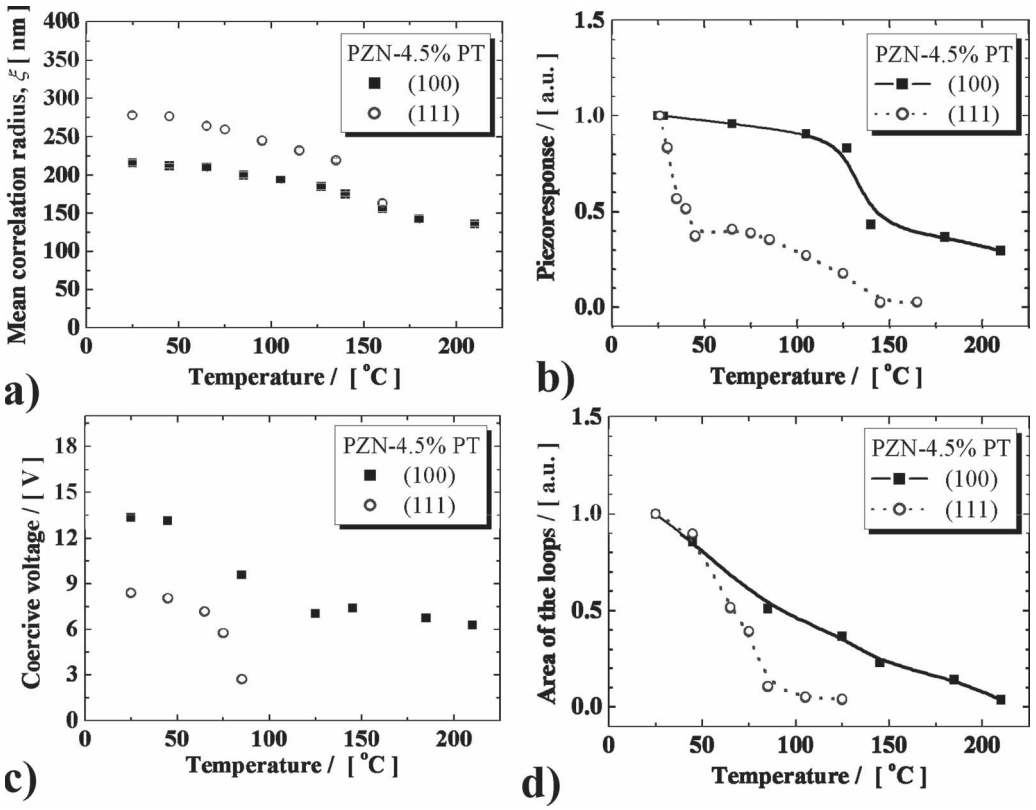

Figure 6. Temperature dependence of a) correlation length, b) static polarization amplitude, c) effective coercive bias and d) switchable polarization obtained from local PFM hysteresis loops for PZN-4.5%PT single crystals of both (100) and (111) orientations.

(compare temperature behavior of static and dynamic polarization for (100) and (111) surfaces shown in Figure 6b and d. However, within the experimental error (finite sensitivity, non-zero probing bias) the corresponding transition temperatures are different. This suggests that the static and dynamic polarization components coexist, as illustrated in **Figure 7**. The switchable dipoles within the static domains have a broad angular distribution $F(\theta)$, where θ is the angle with surface normal. Denoting the corresponding first and second order moments as S and D, for positive labyrinthine domains we have $S = 0$ and $D/S \sim 1$–10, whereas for negative ones we have $S = \pi$ and $D/S \sim 1$–10. In other words, the disorder is large, but there is a preferred polarization orientation (contrary to the spherically-symmetric models of relaxors). In comparison, in classical ferroelectrics the disorder is small, $S = 0$ and $D/S = 0$ for positive domains and $S = \pi$ and $D/S = 0$ for negative domains. The local poling (if in the positive direction) results in decrease of D/S, and hence increase of overall response (can be by a factor of ~4–10).

This behavior can be related to the surface-induced mesoscopic phase transition driven by

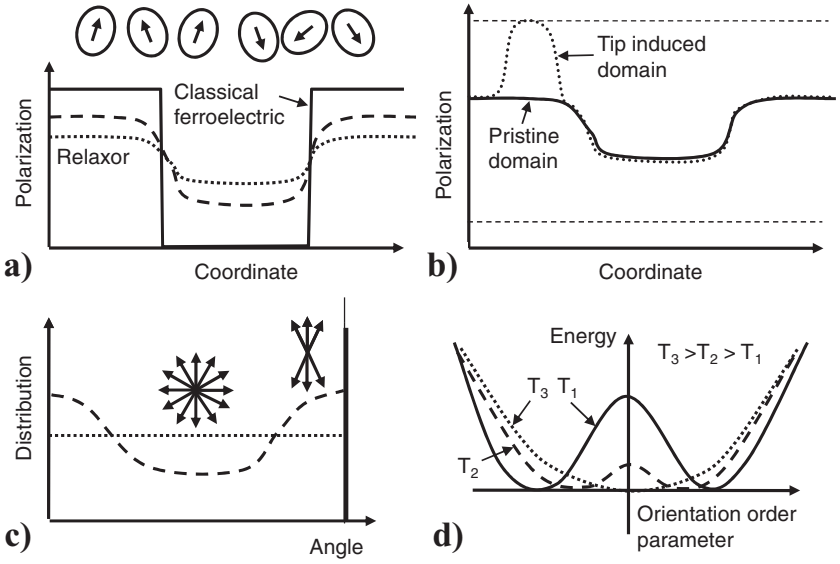

Figure 7. Schematic representation of surface-induced mesoscopic phase transition on relaxor surfaces. a) Polarization distribution in classical ferroelectric (solid line) and relaxor at two different temperatures (broken and dotted lines). While in ferroelectrics the domain pattern is hard and formed by strongly interacting unit cell dipoles, in relaxors the basic building blocks are weakly interacting PNR dipoles with broad angular distribution leading to diffuse domain walls and sinusoidal polarization states. b) Application of strong tip bias narrows the distribution of PNRs resulting in large piezoresponse that relaxes with time in a spatially uniform fashion. c) Surface phase transition corresponds to a change of the rotationally invariant (Heisenberg) to transversally isotropic (Ising) distribution. d) Corresponding free energy vs. order parameter.

strain relaxation, electric fields, or more complex effects. Note that electrostatic interactions will favor the in-plane dipole orientation, rather then out of plane. Hence, we believe that the presence of the surface breaks the symmetry between possible polarization orientations in PNRs due to elastic interactions (either direct, or due to random field-induced piezostrain). This favors dipole orientation up and down, resulting in transition from "cubic" to "tetragonal" phase. The schematic is shown in Figure 7. The associated lattice deformations are small, and hence the phase is "cubic". The electrical interaction results in secondary breaking of symmetry in plane and formation of classical 180° domain pattern.

2.4. Modelling

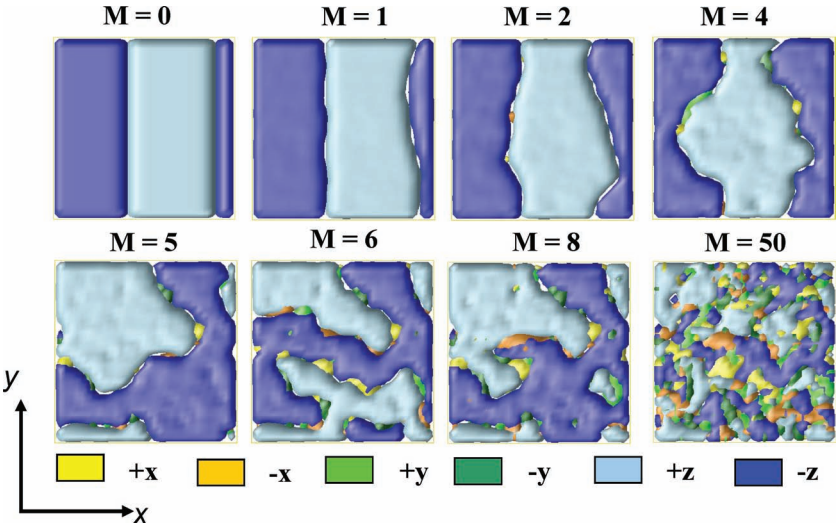

Figure 8. Phase field modeling of domain structure evolution with frozen disorder as a function of disorder strength.

The observed polarization behaviors on the surface of relaxor material raise a number of fundamental questions on their physical origins. Note that the ~100–300 nm length scale of the labyrinthine domains is well outside the range of applicability of both diffuse scattering and optical microscopy based methods, and hence can be detected only by PFM. The classical models of the relaxor state[6,7,59–62] simply do not provide any rationalization of observed behavior (albeit these can rationalize the behavior of the dynamic polarization component). Below, we combine the phase-field modeling and analytical Ginzburg-Landau based theory to rationalize (if not quantify) observed behavior, including (a) absence of classical ferroelectric domains, (b) slow polarization dynamics, and (c) nature of the labyrinthine static polarization component.

As a first step in analysis, we explore the role of field disorder on the domain structure in a classical ferroelectric. Briefly, we consider the prototypical phase of rhombohedral ferroelectric described by a polarization field, and introduce the defect effects as built-in random fields of various magnitudes. The domain structure is then determined by solving the time-dependent Ginzburg-Landau (TDGL) equation

$$\frac{\partial P_i^G\left(x^G,t\right)}{\partial t} = -K\frac{\delta F}{\delta P_i^G\left(x^G,t\right)},\ i=1,2,3 \qquad (1)$$

where K is the kinetic coefficient related to the domain mobility and t is time. The parameters are taken as that for $BiFeO_3$ and have been previously summarized.[63]

The evolution of the initially flat domain wall as a function of disorder M (defined as on-site built-in random field[64]) is shown in **Figure 8**. For small disorder magnitudes, the domain wall roughens due to the preferential pinning on the defects, and may develop small pockets of polarization with different orientation at the interface. For higher disorders (M = 3–7), the fluctuations on domain wall position exceed domain size, resulting in meandering structure. However, the preferential up and down domain states (as stabilized by strain) persist. Finally, for large disorder (M = 50) the system falls apart in the chaotic domain mixture.

This behavior can be understood from simple consideration of domain structure stability in the presence of field disorder, following classical Imry–Ma arguments.[65] For random field defects with strength v (difference in the energy for 2 orientations of polarization) and density $1/D^3$, the domain of the size L contains $(L/D)^3$ defects, and $(L/D)^{3/2}$ defects are aligned, leading to an energy gain $(L/D)^{3/2}v$. For smooth domain walls, the wall energy per domain is σL^2, where σ is the surface tension of the boundary). Hence, equilibrium domain size is $L_o = D^{-3}(v/\sigma)^2$ and corresponding energy density is $U_M = \sigma^3 D^3 v^{-2}$. In comparison, the energy density of a single-domain state is $U_S = v/D^3$. Hence, the single domain state is metastable at $v > \sigma D^2$.

The phase-field modeling results and the scaling arguments above suggest that the presence of the random field defects destabilizes the single-domain states, and leads to the rapid decrease of the domain size. The slow dynamics of these domains is directly responsible for the relaxation behavior in the induced polarization and hysteresis loops observed above the transition temperature. However, these domains cannot account for the periodic domain patterns with characteristic 100–300 nm length that are observed ubiquitously in ergodic relaxors, and coexist with macroscopic domains in the non-ergodic systems.

In explaining the origin of these patterns, we note that some authors[66] introduced single- and two order parameter free energies in which the length appears only in the form of the standard gradient terms. For these models, the characteristic domain size appears typically due to the presence of the characteristic length in the system.[67,68] Here, the observed instability of the ferroelectric wall suggests that the renormalized energy is negative. Correspondingly, the higher-order terms in free energy expansion become relevant,[68] and should be included for the description of the long-order correlations between the next nearest neighbors, while the second derivative coefficients reflects correlations between the nearest neighbors. Within the framework of the continuous theory these gradient terms should be included into the free energy functional expansion on the polarization P_3 powers:

$$F \approx \int_0^L dz \int_{-\infty}^{\infty} dxdy \left(\frac{\alpha_B(T)}{2} P_3^2 + \frac{\beta}{4} P_3^4 + \frac{\gamma}{6} P_3^6 - P_3 \frac{E_3^d}{2} + \sum_{i=1,2,3} \left(\frac{\delta_i}{2} \left(\frac{\partial P_3}{\partial x_i} \right)^2 + \frac{g_i}{2} \left(\frac{\partial^2 P_3}{\partial x_i^2} \right)^2 \right) + \frac{\lambda_i}{2} \cdot P_3^2 \left(\frac{\partial P_3}{\partial x_i} \right)^2 \right) + \frac{\alpha_S(T)}{2} \int_{-\infty}^{\infty} dxdy \; P_3^2 \big|_{z=0} \quad (2)$$

The first integral in (2) is the bulk energy and the second one is the surface energy related to the non-electroded surface $z = 0$.

Note that in what follows we are interested in the intrinsic scale of the labyrinthic modulation, which we believe is weakly affected by the random electric fields. This assumption is justified, since the size of the PNR and random field fluctuations is of the order of several or several tens of nm, and the period of labyrinthic structures is above 100 nm. This allows us not to consider the interaction of polarization with random electric fields in the expansion (2) and regard L as a longitudinal correlation length, if the latter is noticeably smaller than the relaxor sample thickness. Depolarization field E_3^d originates near the relaxor surface due to the incomplete external screening of the nanocluster polarization by the space charge accommodated above/in the contamination layers of thickness H that is typically not more than several lattice constants.

Coefficients of the bulk and surface energies, $\alpha_B(T) = \alpha_{TB}(T - T_B)$ and $\alpha_S(T) = \alpha_{TS}(T - T_S)$, explicitly depend on temperature T. The coefficient β may be positive or negative depending upon the transition order and γ is positive. The signs of all other coefficients are defined from following argumentation. The second derivative coefficients g_i reflect correlations between the nearest neighbors, and the forth derivatives δ_i the correlations of the next neighbors. In relaxor systems (e.g., in PZN-PT with low concentration of the ordered component, say less than 10%), these cannot be the nearest neighbors, so their interaction strength is described by the forth order correlation term δ_i. Thus positive forth-derivative gradient coefficients $\delta_i > 0$ reflect the long-range dipole correlations between PT unit cells, which tend to order the system. The long-range correlations between the nearest neighbors are weak, so the second-derivative gradient coefficients are negative $g_i < 0$.

Substituting polarization Fourier image $\tilde{P}_3(\mathbf{k}, z) = P_0(\mathbf{k}) + p(\mathbf{k}, z)$ into equation of state obtained from minimization of (2) and linearizing it with respect to p, we derived that transverse {x,y} modulation vector as:

$$k_L(T) = \sqrt{-\frac{\delta}{2g} - \sqrt{\frac{\delta^2}{4g^2} - \frac{\alpha_R(T)}{g}}} \quad (3)$$

In Equation 3 we assumed the natural isotropy of the relaxor in the transverse x and y directions (i.e., $\delta_1 = \delta_2 = \delta$, $g_1 = g_2 = g$ and $\lambda_1 = \lambda_2 = \lambda$), in contrast to incommensurate ferroelectrics, which are typically uniaxial. Thus not only the gradient terms $\delta > 0$ and $g < 0$ in the free energy (2) determine the length scale of the modulation (3), but also the coefficient $\alpha_R(T)$ can be renormalized by surface influence and depolarization field as[69,70]:

$$\alpha_R(T) \approx \alpha(T) + \frac{2\alpha_S(T)}{L} + \frac{1}{\varepsilon_0 \varepsilon_{33}^b} \left(1 - \frac{\varepsilon_{33}^g L}{\varepsilon_{33}^g L + \varepsilon_{33}^b H} \right) \quad (4)$$

The thickness of contamination layer is H, its permittivity is ε_{33}^g; ε_{33}^b is the background permittivity of relaxor, ε_0 is the universal dielectric constant. In the linear approximation the intrinsic modulation exists in the temperature range $T_C < T < T_L$, where the "ferroelectric" transition temperature $T_C = T_B + T_S \frac{\alpha_{TS}}{L\alpha_{TB}} - \frac{1}{\varepsilon_0 \varepsilon_{33}^b} \left(1 - \frac{\varepsilon_{33}^g L}{\varepsilon_{33}^g L + \varepsilon_{33}^b H} \right)$ and the modulation temperature $T_L = T_C + \frac{\delta^2}{4g(\alpha_{TB} + \alpha_{TS} L^{-1})}$, at that $k_L^2(T_C) = 0$ and $k_L^2(T_L) = -\frac{\delta}{2g}$. The temperatures are renormalized by surface influence and depolarization field effect.

Note, that linearized solution (3) is qualitatively and semi-quantitatively valid in the vicinity of T_L, where the modulation is "soft" or "harmonic"; it becomes quantitatively incorrect with decreasing temperature, since the modulation becomes "harder", and principally invalid when $T \to T_C$, since the solution tends to zero ($k_L^2(T_C) = 0$) instead of giving some constant value (compare with the situation in the incommensurate ferroelectric films). Nonlinear solution, denoted as $k_{NL}(T)$, is derived in the Supporting Information section. In contrast to linearized solution (3), $k_{NL}(T)$ depends on all the coefficients involved into the free energy (2). Polarization value, corresponding to the solution (3)-(4) is $p_k^2(T) = -\frac{4}{\lambda}\left(\delta + 2gk^2(T)\right)$.

With the inclusion of random electric field defects the transverse axially-indifferent modulation becomes the chaotic one and the period $q(T) = \frac{2\pi}{k(T)}$ should be regarded as transverse correlation radius and at temperature-dependent domain pattern near the surface mimics the labyrinth domain structures. Qualitative explanation of the striking fact can be found in the papers by Bjelis et al.,[71,72] where it was shown that the functional (2) minimization leads to non-integratable problem with chaotic phase portrait, and that periodic solutions are isolated trajectories at the phase portrait in and are physically trains of commensurate and incommensurate domains of various periods. Note that Bjelis et al. considered the uniaxial case.

Temperature dependences of the correlation length for relaxor systems: PLZT-8%, PLZT-9.5%, PZN-4.5%PT (100) and PZN-4.5%PT (111) are shown in **Figure 9** in comparison with experimental data. Parameters used in calculations are summarized in the **Table 1**. Tabulated parameters for incommensurate-commensurate normal ferroelectric $Sn_2P_2(Se,S)_6$ are shown for comparison. Actually the difference in the parameters α_T (two or three orders lower than in $Sn_2P_2Se_6$) and the gradient term g (two orders higher than in $Sn_2P_2Se_6$) play the decisive role. The difference in g may be reasonable, because relaxors typically have much broader domain walls than the ordered ferroelectrics have.[73] The difference in α_T originated from the surface and depolarization effect renormalization (see Equation. 4). To summarize the modeling section, the absence of the classical ferroelectric domains and dynamic polarization

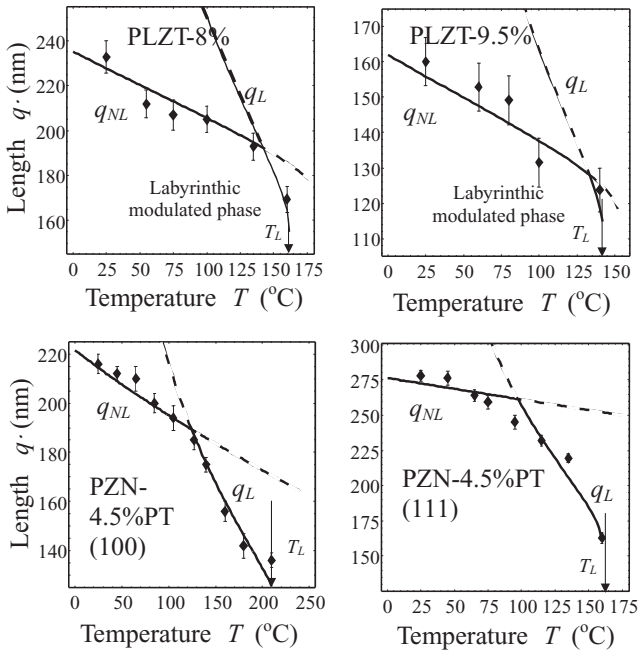

Figure 9. Temperature dependence of the correlation length for relaxor systems: a) PLZT-8%, b) PLZT-9.5%, c) PZN-4.5%PT (100), and d) PZN-4.5%PT (111). Symbols are experimental data, solid curves are $q_L(T)$ and $q_{NL}(T)$ calculated from Equations 3 and 4, respectively. Parameters used in calculations are summarized in Table 1.

component is consistent with the existing theories of relaxor state. The labyrinthine patterns can be explained by the presence of higher-order term in free-energy expansion that naturally gives rise to the polarization modulations. Note that the length scale of these modulations and the smallness of associated lattice deformations severely limit the efficacy of scattering-based studies. Alternatively, these can be a result of the near-surface electric field and strain relaxation. The likelihood of this field-based explanation is limited, since these domains are not affected by electric fields (although they may be due to the screening by mobile polarization component). The ferroelastic model also does not immediately explain the presence of characteristic length scale.

3. Conclusions

To summarize, we have studied the mesoscopic polarization ordering in several families of relaxors. The combination of imaging and spectroscopy data indicates the presence of two component order parameters with dynamic and static components, respectively. The symmetry breaking in the surfaces results in the formation of non-fractal ordered structures with characteristic length scale. These domain structures are only weakly sensitive to electric field, and gradually disappear with increasing temperature. The dynamic polarization component is (within the experimental error) uniform within the material and can be easily manipulated by the field of a PFM tip. The formed domain relaxes uniformly (rather than through the wall motion) and penetrates the material only by few tens of nanometers. Both static and dynamic polarization components exist well above the temperature of maximum bulk dielectric constant, and their temperature behavior is strongly dependent on crystallographic plane. The possible origins of these patterns are analyzed and attributed to the negative wall energy due to the contribution of higher-order gradient terms in the free energy expansion.

With respect to the physics of relaxor compounds, this study clearly illustrates the importance of mesoscopic polarization patterns that are until now overlooked by major theories of relaxor states. An obvious and open question is the relation of these observations to recent neutron based studies illustrating the presence of static and dynamic order parameters in relaxors,[76] as well as reports on local strains and domain like dynamics[77] and surface layers.[51]

Finally, we note that many of the observed behaviors exist in other disordered systems, ranging from structural to spin glasses. In particular, mesoscopic phase separation and two order parameters were introduced to describe the properties of cooled water.[78] However, these systems present significant challenges for mesoscopic observations due to the lack of appropriate imaging tools. Ferroelectric relaxors provide a convenient model system, in which the dipole reorientation does not change the underlying crystallographic lattice, and hence is (potentially) reversible. At the same time, the strong coupling between polarization and strain (reversible lattice deformation) allows the polarization dynamics to be studied. The results of these studies can be extended to other disordered systems such

Table 1. Values of the free energy coefficients used in calculations (columns 2-5) in comparison with data for incommensurate (column 6) and commensurate (column 7) ferroelectrics.[74,75]

Coefficient	PLZT-8% La	PLZT-9.5% La	PZN-4.5% PT (111)	PZN-4.5% PT (100)	Normal incommensurate FE ($Sn_2P_2Se_6$)	Normal commensurate FE ($Sn_2P_2S_6$)
α_T, J m C^{-2} K^{-1}	1.2×10^4	1.6×10^4	3.8×10^3	5.0×10^3	1.6×10^6	1.6×10^6
β, J m^5 C^{-4}	-8×10^8	-8×10^8	-8×10^8	-8×10^8	-4.8×10^8	7.4×10^8
γ, J m^9 C^{-6}	8×10^{10}	8×10^{10}	8×10^{10}	8×10^{10}	8.5×10^{10}	3.5×10^{10}
δ, J m^3 C^{-2}	-2.4×10^{-9}	-1.4×10^{-9}	-7.9×10^{-10}	-6.8×10^{-10}	-5.7×10^{-10}	$(1.4–1.6) \times 10^{-10}$
g, J m5 C^{-2}	7.20×10^{-25}	2.15×10^{-25}	2.56×10^{-25}	1.04×10^{-25}	1.8×10^{-27}	Indetermined
λ, J m^7 C^{-4}	4.9×10^{-7}	2.8×10^{-7}	1.8×10^{-7}	1.8×10^{-7}	$(1.2–1.3) \times 10^{-8}$	Indetermined
T_L, °C	162	143	160	222	$T_{IC} = -52$	Indetermined
T_L, °C	0	70	150	155	–80	64

as structural glasses, polymers (in which the dynamics are irreversible) and spin- and cluster glasses (in which mapping local magnetization is still a challenge).

4. Experimental Section

Materials: Our experiments have been carried out on PLZT ceramics sintered in Jožef Stefan Institute, Slovenia.[79] PZN-4.5%PT single crystals were provided by Dr. Paul Rehrig (TRS Ceramics, USA) and oriented along (111) and (001) planes using the conventional Laue setup. The ceramics and oriented crystals were polished to the desired thicknesses by using several abrasives in the following order: (a) silicon carbide paper, (b) diamond paste (3 μm, 1 μm and 0.25 μm), (c) colloidal-silica aqueous suspension (~0.05 μm). Submicron polishing was performed only when required by certain experiments, such as domain studies. The final surface area of the polished samples used in these experiments varied from 5 mm × 5 mm, while the final thicknesses were in the range 100–200 μm.

Macroscopic Measurements: The macroscopic hysteresis loops were measured in a sinusoidal electric field at a frequency of 50 Hz and at amplitudes up to 10 kV cm^{-1}. The measurements were carried out in the temperature range from 25 to 130 °C in the home-made setup.

PFM and SS-PFM: Commercial scanning probe systems (NT-MDT, Ntegra Aura and Agilent 5420) equipped with additional function generator and lock-in amplifier (Yokogawa FG120, Stanford Research SR-830) were used for PFM measurements. In this method, a sharp conductive tip in contact with the surface is periodically biased, and bias-induced surface displacements are translated into the mechanical motion of the tip.[80] In piezoresponse switching spectroscopy, the dc bias offset applied to the tip is changed to follow a triangular wave, and the nucleation and growth of the ferroelectric domain below the tip are reflected in the variation of the effective piezoresponse. The resulting hysteresis loops contain information on ferroelectric switching at a single location. We used hard cantilevers (NCHR, 40 N m^{-1}, Nanoworld) without coating and frequency 50 kHz for both imaging and hysteresis loop acquisition.

Supporting Information

Supporting Information is available from the Wiley Online Library or from the author.

Acknowledgements

We thank Prof. A. Tagantsev for valuable discussions and Dr. S. Drnovsek for the assistance with temperature measurements. The research was supported in part (S.V.K.) by the Division of Scientific User facilities, DOE BES (project CNMS2009-090). D.K. and A.K. are grateful to the Portuguese Foundation for Science and Technology (FCT) for the support within the PhD grant SFRH/BD/22391/2005 and project PTDC/FIS/81442/2006. A.B. and Z.-G.Y. acknowledge U.S. Office of Naval Research (N00014-06-0166) and the Natural Science & Engineering Research Council of Canada (NSERC) for the support.

Received: December 8, 2010
Revised: February 8, 2011
Published online: April 12, 2011

[1] K. Binder, A.P. Young, *Rev. Mod. Phys.* **1986**, *58*, 801.
[2] V. Wadhawan, *Introduction to Ferroic Materials*, Gordon and Breach, New York **2000**.
[3] W. Kleemann, *Int. J. Mod. Phys.* **1993**, *7*, 2469.
[4] G. A. Smolenskii, *J. Phys. Soc. Jpn.* **1970**, 28, 26.
[5] C. A. Angell, *J. Phys. Chem. Solids* **1988**, *49*, 863.
[6] G. Blatter, M. V. Feigelman, V. B. Geshkenbein, A. I. Larkin, V. M. Vinokur, *Rev. Mod. Phys.* **1994**, *66*, 1125.
[7] R. Pirc, R. Blinc, *Phys. Rev. B* **1999**, *60*, 13470.
[8] a) G. A. Smolensky, V. A. Isupov, *Sov. Phys. Tech. Phys.* **1954**, *24*, 1375; b) G. A. Smolensky, A. I. Agranovskaya, *Sov. Phys. Tech. Phys.* **1958**, *3*, 1380.
[9] G. A. Smolensky, V. A. Bokov, V. A. Isupov, N. N. Krainik, R. E. Pasynkov, A. I. Sokolov, N. K. Yushin, *Ferroelectrics and Related Materials*, Gordon and Breach, New York **1981**.
[10] G. Burns, F.H. Dacol, *Phys. Rev. B* **1983**, *28*, 2527.
[11] L. E. Cross, in *Ferroelectric Ceramics* (Eds. N. Setter, E. Colla), Birkhausen, Berlin **1993**.
[12] A. A. Bokov, Z.-G. Ye, *J. Mater. Sci.* **2006**, *41*, 31.
[13] Z. Kutnjak, J. Petzelt, R. Blinc, *Nature* **2006**, *441*, 956.
[14] A. K. Jonscher, *Dielectric Relaxation in Solids*, Chelsea Dielectric Press, **1983**.
[15] O. Kircher, B. Schiener, R. Bohmer, *Phys. Rev. Lett.* **1998**, *81*, 4520.
[16] G. Y. Xu, P. M. Gehring, G Shirane, *Phys. Rev. B* **2005**, *72*, 214106.
[17] I. Grinberg, Y. H. Shin, A. M. Rappe, *Phys. Rev. Lett.* **2009**, *103*, 197601.
[18] J. Toulouse, F. Jiang, O. Svitelskiy, W. Chen, Z.-G. Ye, *Phys. Rev. B* **2005**, *72*, 184106.
[19] M. Matsuura, K. Hirota, P. M. Gehring, Z.-G. Ye, W. Chen, G. Shirane, *Phys. Rev. B* **2006**, *74*, 144107.
[20] See, e.g., T. Egami, *Annu. Rev. Mater. Res.* **2007**, *37*, 297 and references therein.
[21] G. H. Haertling, C. E. Land, *J. Am. Ceram. Soc.* **1971**, *1*, 54.
[22] a) S.-E. Park, T. R. Shrout, *J. Appl. Phys.* **1997**, *82*, 1804; b) D. Viehland, A. Amin, J.-F. Li, *Appl. Phys. Lett.* **2001**, *79*, 1006.
[23] S. B. Vakhrushev, A. A. Naberezhnov, B. Dkhil, J.-M. Kiat, V. Shvartsman, A. Kholkin, A. Ivanov, in *Fundamental Physics of Ferroelectrics 2003,* AIP Conf. Proc. **2003**, *677*, 74.
[24] F. Bai, J.-F. Li, D. Viehland, *Appl. Phys. Lett.* **2004**, *85*, 2313.
[25] A. L. Kholkin, I. K. Bdikin, V. V. Shvartsman, in "*Scanning Probe Microscopy of Functional Materials: Nanoscale Imaging and Spectroscopy*", (Eds. A. Gruverman, S. Kalinin, Springer, New York **2010**.
[26] V. V. Shvartsman, A. L. Kholkin, *J. Appl. Phys.* **2007**, *101*, 064108.
[27] S. V. Kalinin, B. J. Rodriguez, S. Jesse, A. N. Morozovska, A. A. Bokov, Z.-G. Ye, *Appl. Phys. Lett.* **2009**, *95*, 142902.
[28] A. Gruverman, A. Kholkin, *Rep. Prog. Phys.* **2006**, *69*, 2443.
[29] S. V. Kalinin, A. N. Morozovska, L.-Q. Chen, B. J. Rodriguez, *Rep. Prog. Phys.* **2010**, *73*, 056502.
[30] A. Gruverman, O. Auciello, H. Tokumoto, *Annu. Rev. Mat. Sci.* **1998**, *28*, 101.
[31] H. Y. Guo, J. B. Xu, L. H. Wilson, Z. Xie, E. Z. Luo, S. B. Hong, H. Yan, *App. Phys. Lett.* **2002**, *81*, 715.
[32] A. Roelofs, U. Bottger, R. Waser, F. Schlaphof, S. Trogisch, L. M. Eng, *Appl. Phys. Lett.* **2000**, *77*, 3444.
[33] A. L. Kholkin, D. A. Kiselev, I. K. Bdikin, A. Sternberg, B. Dkhil, S. Jesse, O. Ovchinnikov, S. V. Kalinin, *Materials* **2010**, *3*, 4860.
[34] F. Bai, J.-F. Li, D. Viehland, *Appl. Phys. Lett.* **2004**, *85*, 2313.
[35] S. V. Kalinin, B. J. Rodriguez, J. D. Budai, S. Jesse, A. N. Morozovska, A. A. Bokov, Z.-G. Ye, *Phys. Rev. B* **2010**, *81*, 064107.
[36] A. Hubert, R. Schafer, *Magnetic Domains: The Analysis of Magnetic Microstructures*, Springer, Berlin, **1998**.
[37] D. A. Kiselev, *Piezoresponse Force Microscopy of Ferroelecric Relaxors*, PhD thesis, University of Aveiro, **2010**.
[38] D. A. Kiselev, I. K. Bdikin, E. K. Selezneva, K. Bormanis, A. L. Kholkin, *J. Phys. D. Appl. Phys.* **2007**, *40*, 7109.
[39] V. V. Shvartsman, A. L. Kholkin, *Phys. Rev.B* **2004**, *69*, 014102.
[40] K. S. Wong, J. Y. Dai, X. Y. Zhao, H. S. Luo, *Appl. Phys. Lett.* **2007**, *90*, 162907.
[41] T. Tybell, P. Paruch, T. Giamarchi, J. M. Triscone, *Phys. Rev. Lett.* **2002**, *89*, 097601.

[42] A. Agronin, M. Molotskii, Y. Rosenwaks, G. Rosenman, B. J. Rodriguez, A. I. Kingon, A. Gruverman, *J. Appl. Phys.* **2006**, *99*, 104102.
[43] B. J. Rodriguez, R. J. Nemanich, A. Kingon, A. Gruverman, S. V. Kalinin, K. Terabe, X. Liu, K. Kitamura, *Appl. Phys. Lett.* **2005**, *86*, 012906.
[44] X. Y. Liu, K. Kitamura, K. Terabe, *Appl. Phys. Lett.* **2006**, *89*, 142906.
[45] Y. Kan, X. Lu, X. Wu, J. Zhu, *Appl. Phys. Lett.* **2006**, *89*, 262907.
[46] A. L. Kholkin, D. K. Kiselev, I. K. Bdikin (unpublished).
[47] R. Landauer, *J. Appl. Phys.* **1957**, *28*, 227.
[48] M. Molotskii, *J. Appl. Phys.* **2003**, *93*, 6234.
[49] A. N. Morozovska, S. V. Svechnikov, E. A. Eliseev, S. Jesse, B. J. Rodriguez, S. V. Kalinin, *J. Appl. Phys.* **2007**, *102*, 114108.
[50] S. V. Kalinin, A. Gruverman, B. J. Rodriguez, J. Shin, A. P. Baddorf, E. Karapetian, M. Kachanov, *J. Appl. Phys.* **2005**, *97*, 074305.
[51] G. Xu, H. Hiraka, K. Ohwada, G. Shirane, *Appl. Phys. Lett.* **2004**, *84*, 3975.
[52] Z. Xu, D. Viehland, P. Yang, D. A. Payne, *J. Appl. Phys.* **1993**, *74*, 3406.
[53] a) C. A. Randall, D. J. Barber, P. Groves, R. W. Whatmore, *J. Microsc.*, **1987**, *145*, 275; b) K. J. Stringer, C. A. Randall, *J. Am. Cer. Soc.* **2007**, *90*, 1802.
[54] D. Kan, L. Palova, V. Anbusathaiah, C. J. Cheng, S. Fujino, V. Nagarajan, K. M. Rabe, I. Takeuchi, *Adv. Func. Mat.* **2010**, *20*, 1108.
[55] E. V. Balashova, A. K. Tagantsev, *Phys. Rev. B* **1993**, *48*, 9979.
[56] A. N. Salak, V. V. Shvartsman, M. P. Seabra, A. L. Kholkin, V. M. Ferreira, *J. Phys.: Cond. Matter* **2004**, *16*, 2785.
[57] M. Ozgul, K. Takemura, S. Trolier McKinstry, C. A. Randall, *J. Appl. Phys.* **2001**, *89*, 5100.
[58] E. Husson, M. Chubb, A. Morell, *Mat. Res. Bull.* **1988**, *23*, 357.
[59] A. E. Glazounov, A.K. Tagantsev, *Phys. Rev. B* **1996**, *53*, 11281.
[60] V. Westphal, W. Kleemann, M. Glinchuk, *Phys. Rev. Lett.* **1992**, *68*, 847.
[61] B. E. Vugmeister, H. Rabitz, *Phys. Rev. B* **2000**, *61*, 14448.
[62] B. E. Vugmeister, M. Glinchuk, *Rev. Mod. Phys.* **1990**, *62*, 993.
[63] B. J. Rodriguez, S. Choudhury, Y. H. Chu, A. Bhattacharyya, S. Jesse, K. Seal, A. P. Baddorf, R. Ramesh, L.-Q. Chen, S. V. Kalinin, *Adv. Func. Mater.* **2009**, *19*, 2053.
[64] L. Q. Chen (unpublished).
[65] Y. Imry, S. Ma, *Phys. Rev. Lett.* **1975**, *35*, 1399.
[66] S. Prosandeev, M. Panchelyuga, S. Raevskaya, I. Raevski, *Appl. Phys. Lett.* **2007**, *91*, 242904.
[67] C. Kittel, *Phys. Rev.* **1946**, *70*, 965.
[68] G. H. F. van Raaij, K. J. H. van Bemmel, T. Janssen, *Phys. Rev. B* **2000**, *62*, 3751.
[69] A. N. Morozovska, E. A. Eliseev, JianJun Wang, G. S. Svechnikov, Yu. M. Vysochanskii, V. Gopalan, L. Q. Chen, *Phys. Rev. B* **2010**, *81*, 195437.
[70] A. N. Morozovska, E. A. Eliseev, S. V. Svechnikov, A. D. Krutov, V. Y. Shur, A.Y. Borisevich, P. Maksymovych, S. V. Kalinin, *Phys. Rev. B* **2010**, *81*, 205308.
[71] V. Dananic, A. Bjelis, *Phys. Rev. E* **1994**, *50*, 3900.
[72] V. Dananic, A. Bjelis, M. Rogina, E. Coffou, *Phys. Rev. A* **1992**, *46*, 3551.
[73] W. Kleemann, *J. Mater. Sci.* **2006**, *41*, 129.
[74] Yu. M. Vysochanskii, M. M. Mayor, V. M. Rizak, V. Yu. Slivka, M. M. Khoma, *Sov. Phys. JETP* **1989**, *68*, 72.
[75] K. J. Stringer, C. A. Randall,*J. Am. Cer. Soc.* **2007**, *90*, 1802
[76] C. Stock, L. Van Eijck, P. Fouquet, M. Maccarini, P. M. Gehring, G. Y. Xu, H. Luo, X. Zhao, J.F. Li, D. Viehland, *Phys. Rev. B* **2010**, *81*, 144127.
[77] E. Dulkin, B. Mihailova, M. Gospodinov, E. Mojaev, M. Roth, *J. Phys. C* **2010**, *22*, 222201.
[78] H. Tanaka, *J. Chem. Phys.* **1999**, *111*, 3163.
[79] M. Kosec, D. Kolar, *J. Physique* **1986**, *47*, 379.
[80] N Balke, I. Bdikin, S. V. Kalinin, A. L. Kholkin, *J. Am. Ceram. Soc.* **2009**, *92*, 1629. N. Balke